HHS Public Access

Author manuscript

Methods Cell Biol. Author manuscript; available in PMC 2021 February 22.

Published in final edited form as:

Methods Cell Biol. 2019 ; 153: 25–42. doi:10.1016/bs.mcb.2019.03.015.

Measurement of cytoplasmic and cilioplasmic calcium in a single living cell

Rinzhin T. Sherpa[a], **Rajasekharreddy Pala**[a], **Ashraf M. Mohieldin**[a], **Surya M. Nauli**[a,b,*]

[a]Department of Biomedical & Pharmaceutical Sciences, Chapman University School of Pharmacy (CUSP), Chapman University, Irvine, CA, United States

[b]Department of Medicine, University of California Irvine, Irvine, CA, United States

Abstract

Cellular signaling represents an evolution of biological systems to sense external stimuli and communicate extracellular microenvironment to the intracellular compartments. The processes underlying molecular signaling have been widely studied due to their important cellular functions. There are numerous techniques available to quantitate the different molecules involved in cellular processes. Among them, calcium is a ubiquitous signaling molecule involved in many biological pathways. Over time the methods to measure intracellular calcium have advanced to better understand its role as a second messenger. In this chapter, we introduce a method to study a single cilium, a mechanosensor that elicits a calcium signaling cascade. To successfully observe the calcium changes in this thin cylindrical-like projection from the cell surface, we utilize a genetically encoded sensor with a high spatial and temporal resolution. In addition, the probe must be localized to the ciliary compartment in order to observe the intraciliary calcium signaling dynamics. To this end, a cilium targeting genetically encoded indicator is used to observe calcium fluxes in both cytoplasm and cilioplasm.

1 Introduction

Calcium ions (Ca^{2+}) are essential in biological systems. They play important roles as a secondary messenger in regulating vascular tone (Falcone, Kuo, & Meininger, 1993; Johns et al., 1987), neurotransmitter release (Kerr et al., 2000; Sabatini, Oertner, & Svoboda, 2002), muscle contraction (Ebashi & Endo, 1968; Forder, Scriabine, & Rasmussen, 1985; Wier, Cannell, Berlin, Marban, & Lederer, 1987) and immune responses (Ebashi & Endo, 1968; Forder et al., 1985; Wier et al., 1987) among many others. Even the beginning of life requires the spark of Ca^{2+} during fertilization (Ebashi & Endo, 1968; Forder et al., 1985; Wier et al., 1987). Ca^{2+} signaling affects every aspect of a cell's life and death. Just as Ca^{2+} signaling has been conserved throughout evolution, the primary cilium has also been conserved from our primitive ancestors. Cilia are slender microtubule-based organelles that protrude from the apical membrane in most adherent cells (Sorokin, 1962, 1968). However, these non-motile cilia were once thought to be a vestigial cell appendage without any apparent function. That was the consensus until studies looking into a possible

*Corresponding author: nauli@chapman.edu; snauli@uci.edu.

mechanosensory function of the primary cilium proved it to be an essential cellular organelle (Malone et al., 2007; Masyuk et al., 2006; Nauli et al., 2003, 2013, 2008; Praetorius & Spring, 2001, 2003). Praetorius and Spring used a setup of differential interference contrast (DIC) and fluorescent microscopy to observe MDCK (Madin-Darby Canine Kidney) cells incubated with Fluo-4, a fluorescent calcium indicator. Then micropipette suction was applied in order to bend the cilia and detect flow-induced Ca^{2+} changes (Praetorius & Spring, 2001, 2003).

The fluid flow-induced cilium bending initiates an intracellular Ca^{2+} influx followed by global Ca^{2+} increase and sustained membrane hyperpolarization (Praetorius & Spring, 2001, 2003). Since then, other studies have found a mechanosensory complex of polycystins 1 & 2 (PC 1 and PC 2) in the ciliary membrane of the renal epithelia which mediate flow sensation (Jin et al., 2014; Nauli et al., 2003, 2008). The bending of the primary cilium causes conformational change in the PC 1 and the associated PC 2, a transient receptor potential Ca^{2+} channel, is then activated causing an influx of extracellular Ca^{2+} (Delmas et al., 2002; Hanaoka et al., 2000; Nauli et al., 2003; Nauli, Pala, & Kleene, 2016). The influx then triggers the release of Ca^{2+} from the intracellular stores through the stimulation of ryanodine receptors (Nauli et al., 2003; Xu et al., 2006). Other studies have found that the cilia are enriched with critical proteins in signaling pathways like Hedgehog, Wnt and Notch as well as membranous GPCRs (Haycraft et al., 2005; Huang & Schier, 2009; Ishikawa, Thompson, Yates, Marshall, & Marshall, 2012; Pazour, Agrin, Leszyk, & Witman, 2005; Schou, Pedersen, & Christensen, 2015). All these proteins are synthesized in the cytosol and eventually transported to the cilia by intraflagellar transport (IFT) apparatus (Liem et al., 2012; Mukhopadhyay et al., 2010; Pazour, Dickert, & Witman, 1999).

With the function of collecting mechanical and chemical cues from the environmental milieu, the importance and the wide functional coverage of the primary cilia becomes even more apparent when the cilia are defective (Christensen, Clement, Satir, & Pedersen, 2012; Singla & Reiter, 2006). The range of diseases affecting multiple systems in the body due to dysfunctional cilia is called ciliopathies (Kathem et al., 2014; Nauli, Sherpa, Reese, & Nauli, 2016; Pala et al., 2018). As the flow-mediated Ca^{2+} influx can be a functional readout of physiologically relevant cilia function, technologies to study and measure Ca^{2+} changes within the cilia and the cytoplasm are needed.

The challenge of observing live Ca^{2+} levels in the cilia arise due to the size of primary cilia. With a diameter around 200nm and a perpendicular orientation in relation to the cell monolayer, it requires specific setup to visualize the cilium together with the cytoplasm since they are at different planes of view (Jin et al., 2014; Su et al., 2013). In addition to these difficulties, traditional Ca^{2+} indicators also fail to reach the cilioplasm requiring modification of sensors to target the cilia. The exclusion of most cellular components and exogenous compounds, unless specifically designated for the cilia, happens due to a diffusion barrier at the base of the cilia (Breslow, Koslover, Seydel, Spakowitz, & Nachury, 2013; Hu et al., 2010; Satir, 2017). The presence of a barrier between the cytoplasm and cilioplasm was first observed using freeze-fracture electron microscopy by Gilula and Satir in the form of a “ciliary necklace” (Gilula & Satir, 1972). This detailed molecular composition of this transition zone at the base of cilia remains to be established. Nonetheless

it is interesting to find that mutated proteins involved in ciliopathies localize to the ciliary transition zone and might be necessary for shuttling biomolecules (Delous et al., 2007; Fliegauf et al., 2006; Mollet et al., 2005; Otto et al., 2005, 2003; Valente et al., 2010; Williams, Masyukova, & Yoder, 2010; Williams, Winkelbauer, Schafer, Michaud, & Yoder, 2008). The consensus is that while some small cytosolic proteins might freely diffuse into the cilia larger molecules or complexes will require a favorable interaction with the transition zone before entering the cilioplasm. To overcome this challenge, researchers have added targeting modules intended to transport the attached cargo into the cilia. Relying on the same strategy, we outline a method of single-cell imaging technique to distinctively visualize Ca^{2+} signaling in the intraciliary compartment and cytosol of a live cell.

2 Choosing Ca^{2+} indicators

Detecting Ca^{2+} fluxes in cells are best studied using Ca^{2+} indicators. With the backing of years of research, there are now a collection of indicators that can be used to examine Ca^{2+} dynamics. There are two main categories of Ca^{2+} indicators: (1) small molecule and (2) genetically encoded calcium indicators (GECIs) (Brini et al., 1994; Cobbold & Rink, 1987; Mank et al., 2008; Miyawaki et al., 1997; Nagai, Sawano, Park, & Miyawaki, 2001; Nakai, Ohkura, & Imoto, 2001; Palmer et al., 2006; Romoser, Hinkle, & Persechini, 1997). Small molecule indicators have superior dynamic range, higher sensitivity and rapid response kinetics (Pérez Koldenkova & Nagai, 2013; Rudolf, Mongillo, Rizzuto, & Pozzan, 2003).

Small molecule indicators like Fura-2 acetoxymethyl ester (Fura-2AM) are robust, allowing ratiometric measurements that can be easily interpreted and less prone to experimental artifacts (Williams, Fogarty, Tsien, & Fay, 1985). Another key point to consider is to ensure that the affinity for Ca^{2+} (K_d), which can vary among the indicators, is suitable to measure the local Ca^{2+} concentration in the region of interest. Nonetheless, all these depend on the availability of a microscope with the proper setup of emission channels, acquisition features, and motorized filter wheels if ratiometric indicators are used. Even with their advantages, small molecule indicators cannot be used for applications that focus on delineating organelle specific Ca^{2+} changes. Cell-permeant indicators, like Fura-2AM, or ones that require more invasive methods are assumed to be homogeneously distributed in the cytosol after loading. But these indicators face the possibility of being either included or excluded from membrane-enclosed structures in the cell. Since signaling depends on spatial origin and compartmentalization, indicators that can segregate into target organelles are valuable to appreciate the different spatial compartments of signaling.

The other class of indicators is GECI, which are constructed with a Ca^{2+} binding module and one or more fluorophores (Fig. 1). As a general mechanism, in most GECIs Ca^{2+} interacts with the binding domain, conformational changes are transferred to the fluorophores affecting the fluorescence intensity. GECIs require gene transfer, i.e., insertion of the nucleic acid sequence coding for the sensor into the cell line of interest. There are a variety of transduction/transfection methods that can be used for transformation. Once expressed in the cells, the indicator is incorporated in the cellular milieu. This is an advantage over small molecule indicators which require repetitive dye incubation for every

experiment, suffer from dye leakage and prone to cellular toxicity during extended time-lapse experiments.

To address the lack of cellular localization ability of small molecule indicators, an addition of targeting sequence to the GECI can be done. There are GECIs that have been targeted to organelles like mitochondria (Filippin et al., 2005; Palmer et al., 2006), golgi (Griesbeck, Baird, Campbell, Zacharias, & Tsien, 2001), endoplasmic reticulum (Miyawaki et al., 1997; Palmer, Jin, Reed, & Tsien, 2004) and nucleus (Miyawaki et al., 1997). Choosing indicators is strictly determined by the needs of the researcher, and the key characteristics to consider include the dynamic range, affinity (K_d) of the indicator for Ca^{2+}, response kinetics and targeting ability.

In our experiments, we are interested in the primary cilia, which is a cellular projection arising from the cell and plays a sensory role in a variety of specialized cells (Malone et al., 2007; Masyuk et al., 2006; Nauli et al., 2003, 2008). For our purpose, we utilize 5HT6-mCherry-G-GECO1.0 (Fig. 1C, Addgene, Cat. 47500) developed by Su et al. which contains a cilium-targeting sequence (CTS) derived from 5HT6, a serotonin receptor (Berbari, Johnson, Lewis, Askwith, & Mykytyn, 2008), a mCherry marker and the Ca^{2+} sensor G-GECO1 (Zhao et al., 2011). G-GECO1 is a single fluorescent sensor based on G-CaMP3, an iteration of the original G-CaMP. A few G-CaMP3 iterations and their cilia targeting fusions are outlined in Table 1. Like the original G-CaMP, G-GECO1 still retains the circularly permuted enhanced green fluorescent protein (EGFP), calmodulin (CaM) in the C terminal, and myosin light chain (M13 peptide sequence) (Nakai et al., 2001; Tian et al., 2009). When Ca^{2+} binds to the CaM domain, conformational changes due to the Ca^{2+}–CaM–M13 interaction induces a subsequent conformational change in EGFP and a change in fluorescent intensity (Akerboom et al., 2012, 2009; Nakai et al., 2001). This changes the fluorescence intensity of EGFP which can be correlated to Ca^{2+} levels. Like other Ca^{2+} indicators, G-CaMP3 by itself fails to penetrate into the cilioplasm and in order to overcome this challenge a CTS derived from ciliary protein can be used. This strategy allows the cellular transportation machinery to move the CTS-attached sensor to the cilia. Like 5HT6, the intracellular C-tail of fibrocystin (Pkhd1 C1–68) (Follit, Li, Vucica, & Pazour, 2010) and the third cytoplasmic loop of SSTR3 (Berbari et al., 2008) are also CTSs among others used to deliver sensors to the cilia (Follit et al., 2010; Jin et al., 2014). The Ca^{2+} sensor, G-GECO1 has double the dynamic range of G-CaMP3, due to substitutions (K119I, L173Q, S404G, and E430V) in the original G-CaMP3. The increased dynamic range is advantageous for observing ciliary Ca^{2+} with a baseline Ca^{2+} as high as 742 nM (DeCaen, Delling, Vien, & Clapham, 2013). The other advantage of 5HT6-mCherry-G-GECO1.0 is the presence of constant mCherry fluorescent marker independent of Ca^{2+} flux. The mCherry aids in visualization of ciliary movement, correction of artifacts and ratiometric analysis of the data.

3 Experimental setup

3.1 Expression of genetically encoded cilia targeting sensor

5HT6-mCherry-G-GECO1.0 plasmid construction has been outlined by Su et al. (2013). Porcine kidney epithelial cells (LLC-PK1, ATCC CL-101) derived from proximal tubules is grown at 37 °C in Dulbecco’s modified Eagle’s medium containing 10% fetal bovine serum

(FBS) and 1% penicillin-streptomycin hence referred as growth media. After reaching a confluence of 60–70%, the cells are transfected with the 5HT6-mCherry-G-GECO1.0 construct using Jetprime transfection reagent (Polyplus Transfection, Ref. 114–15) according to the manufacturer's instructions and selected using G418 at a concentration of 500μg/mL.

3.2 Cell growth on microwire

After selecting cells that express 5HT6-mCherry-G-GECO1.0, the transfected cells can now be grown on a precision tungsten microwire. Tungsten microwire can be obtained through Luma Metall AB, Sweden. We recommend a high purity wire (Wire quality #823), straightened and electrolytically etched with a final diameter of less than 100μm (Surface finish #42) for the experiment. The preparation of the precision microwire requires coating with type I collagen (50μg/mL in 0.02N acetic acid) to provide a conducive surface for cell attachment and growth. The microwires are then UV sterilized for 30min and mounted on the imaging chamber before seeding cells. Cell growth is monitored continuously for 1–2 days and when the confluency reached ~95–98% low serum media (2% FBS) was added to promote ciliation of the cells. If needed the microwire can be gently rotated to observe the confluency of the cells around the microwire.

4 Fluorescence microscopy

4.1 Overview

Microscopy has permitted an appreciation of molecular level activities in cells. Starting from a simple setup of optical lenses used by pioneer scientists to view simple structures, the microscope has evolved into sophisticated digital imaging systems with increased spatial and temporal resolution for specialized procedures in scientific research. The concurrent development of molecular techniques, innovative approaches and iterative progression of fluorescent proteins have contributed to the breakthrough in our understanding of cellular functions.

Fluorescence is the phenomenon of absorption of electromagnetic radiation and the subsequent release of radiation by a fluorophore. A basic fluorescence microscope functions to irradiate the specimen with a desired and specific band of wavelengths. An illumination source produces a specific wavelength band and passes it through a selective excitation filter. The excitation light then reflects off from a dichroic mirror to the sample. If the specimen fluoresces, the illumination is then emitted back, albeit at a lower energy level in a phenomenon called Stokes shift. The emission is gathered by the objective and passed back through the dichroic mirror into the emission filter, which blocks the unwanted excitation wavelengths. Building on these basic principles, innovative indicator design using molecular approaches have significantly advanced the use of fluorescence microscopy to study cell processes. So, in addition to a suitable fluorescent indicator for experimental needs, a basic prerequisite is the microscope system which should have the capabilities to support required specifications.

4.2 Experimental setup

Our experimental setup consists of two main components.

- **i.** Flow equipment that includes imaging dishes which are standard 35mm plates with a custom-made glass coverslip bottom. For the imaging dishes, a hole is cut out from the bottom of the plate and using a silicone-based glue (Loctite® Clear Silicone Waterproof Sealant; Item#908570) a glass coverslip is attached to the plate. We also have a perfusion pump with variable flow settings and inlet/outlet tubing to allow fluid flow over the microwire (Fig. 2A).
- **ii.** Imaging equipment, which in our case is an inverted fluorescent microscope with accessories for rapid imaging. We use a Nikon Ti-Eclipse outfitted with excitation and emission filter wheels, controlled by a Lambda 10–3 filter changer. In addition, the DG-5 Plus module high-speed wavelength switcher for rapid imaging of two signals, EGFP and mCherry. The software package is NIS-elements and used to interface with the microscope, filter changer and camera as well as conduct data analysis. The setup can capture DIC and fluorescence images. With the okoLab incubator module, the cells can be sustained in a controlled environment of 37 °C, 5% CO_2 and appropriate humidity for long periods if needed. The 5HT6-mCherry-G-GECO1.0 has EGFP with excitation and emission wavelengths of 495 and 515nm, respectively. The mCherry has excitation and emission wavelengths of 587 and 610nm, respectively. The user must adjust the excitation and emission setup to successfully view the signals. Exposure will also need to be adjusted around 200–600ms for rapid imaging while also maintaining satisfactory baseline signal of the EGFP and mCherry.

4.2.1 Flow equipment setup—In our experiment, we use an Instech P720 peristaltic pump in a closed perfusion system with inlet and outlet to the perfusion chamber (Brown & Larson, 2001; Jin et al., 2014; Nauli et al., 2013). The flow chamber from GlycoTech (Cat. 31–001) is arranged as follows from top to bottom (Fig. 2B)

1. base plate with an inlet and outlet port for perfusate flow.
2. silicone gasket that defines the geometry of the flow region to achieve non-turbulence, laminar flow and seals the chamber from potential fluid leakage.
3. glass bottom plate on which the microwire is to be placed.

The components are set up to minimize the use of excessive long tubing; the volume of perfusate is determined empirically; the pump is primed with perfusate before each experiment. Once the transfected cells expressing 5HT6-mCherry-G-GECO1.0 are fully confluent on the microwire, they are placed on the imaging dish. The assembly is then put together as mentioned above providing an inlet and outlet of fluid (Fig. 2). A range of shear-stress from 0.1 to 50 dyne/cm^2 can be used to induce bending of cilia. Assuming the GlycoTech perfusion chamber to be shaped as a cuboid based on the dimensions of the gasket, the flow rate can be adjusted to obtain the desired shear stress using the following formula.

$$\tau_w = \frac{6Q\eta}{a^2 b}$$

where:

τ_w = Wall shear stress (dyne/cm^2)

Q = Volumetric flow rate in (mL/s)

η = Apparent fluid viscosity in (dyne s/cm^2)

a = Chamber height/gasket thickness (cm)

b = Chamber/gasket width (cm)

As a note, at 33–39°C, Dulbecco's Modified Eagle Medium or HEPES has a calculated viscosity of ~0.0076 dyne s/cm^2 (Nauli et al., 2013).

4.2.2 Monitoring experiment—After assembling flow chamber with the microwire inside, place the plate onto the stage. Join the fluid channels to the pump. Eliminate air bubbles and equilibrate the cells for 15–20min. Use brightfield illumination to focus on the edge to the precision microwire at a lower magnification. Switch to a 100× objective to find a cell with cilia. At a 100× objective and correct positioning, side-view imaging should show both the cilium and the cell body at the same time (Fig. 3A). One can switch directly to the fluorescence illumination, using the mCherry signal to find cilia that should possess the 5HT6-mCherry-G-GECO1.0 sensor. As a note, even the cell body will fluoresce because the sensor is produced in the cytosol before being trafficked into the cilioplasm. Due to the random probability of orientation and mostly due to the ~200nm size of the cilium, finding one may remain elusive and might take a while to find a field that captures both the cilioplasm in its full length and the cytoplasm in focus.

After confirming the fluorescence localization and checking to see proper cell morphology, we can start the experiment. To measure the resting Ca^{2+}, start the data acquisition and collect images every ~1–10s for 5min. The pump can be turned on after collecting baseline data. At this time, data can be collected continuously; i.e., no delay data acquisition to view rapid fluxes in Ca^{2+}. The introduction of flow might lead to small movement initially, but that can be resolved with a focal or stage adjustment to ensure the cilium remains visible and in-focus. After the fluid flow data capture, buffer can be exchanged using stopcock valves to introduce new perfusate and simultaneously eliminate the initial circulating buffer (Fig. 3B). To obtain the minimum fluorescence the buffer is replaced with Ca^{2+}-free solution containing 2mM EGTA and 10μM ionomycin. Using tubing with an inner diameter of 0.02 in. (0.5mm) and length of 8 in. (20cm), we get a dead volume of 39mm^3 or 39μL. Complete media exchange in the flow chamber takes about a minute and the same applies to the time for diverting the Ca^{2+} solution to the waste container. After the minimum signal is determined, the cell is challenged with Ca^{2+} (10mM) to obtain a maximum signal. This is to ensure that (1) the system is responding accordingly to the ambient Ca^{2+} concentration and (2) the dynamic range (or K_d) of the Ca^{2+} indicator is within the expected target.

4.2.3 Data analysis—For analysis, a region of interest (ROI) is generated around the cilium using the ROI tool, and a duplicate ROI is placed adjacent to the cilium for background measurement. A separate ROI is created for the cell body as well. The ROI can be adjusted at various time points after fluid flow to account for the cilium bending. The fluorescence signal intensity data from the ROI can be subtracted from the background fluorescence and two steps of normalization (i) against the mCherry and (ii) basal signal intensities applied to the data. EGFP/mCherry images can be generated by taking the ratio of EGFP and mCherry signal intensities and pseudocolored for viewing (Fig. 4).

For quantification, this process is done for all time points in the time series file and exported to a suitable format for statistical analysis. Multiple experiments will confirm the response seen during stimulation with fluid flow. There might be cases with movement artifacts or fluorescent aggregates, appearing in the field of view after flow initiation. These might introduce significant deviations, but with the help of mCherry, we can evaluate the Ca^{2+}-independent signal deviations and determine the viability of the data.

5 Conclusion

A typical experimental result will provide EGFP and mCherry intensities for the cilioplasm and cytoplasm in response to fluid flow over time which can be presented as a time series plot or a comparative bar graph showing Ca^{2+} levels. A plot of the EGFP as a function of time will show an expected increase in signal intensity upon addition of fluid flow. Upon cessation of fluid flow, the increase in EGFP returns to baseline. The treatment with ionomycin/EGTA causes a transient increase due to the extracellular Ca^{2+} entry from the ionomycin-induced pore formation followed by a slow decline in Ca^{2+} signal due to the Ca^{2+} chelator EGTA. Subsequent treatment with higher Ca^{2+} should increase the signal intensity to a level higher than that observed with fluid flow. The presence of mCherry provides the opportunity to apply ratiometric analysis and elimination of Ca^{2+} related artifacts. Moreover, the time-lapse images can be compiled into a movie to observe Ca^{2+} increases in the cilioplasm and cytoplasm.

Acknowledgments

This work has received funding support in part by Congressionally Directed Medical Research Program PR130153, NIH HL131577 and the Chapman University School of Pharmacy.

References

Akerboom J, Chen T-W, Wardill TJ, Tian L, Marvin JS, Mutlu S, et al. (2012). Optimization of a GCaMP calcium indicator for neural activity imaging. Journal of Neuroscience: The Official Journal of the Society for Neuroscience, 32(40), 13819–13840. 10.1523/JNEUROSCI.2601-12.2012.

Akerboom J, Rivera JDV, Guilbe MMR, Malavé ECA, Hernandez HH, Tian L, et al. (2009). Crystal structures of the GCaMP calcium sensor reveal the mechanism of fluorescence signal change and aid rational design. The Journal of Biological Chemistry, 284(10), 6455–6464. 10.1074/jbc.M807657200. [PubMed: 19098007]

Berbari NF, Johnson AD, Lewis JS, Askwith CC, & Mykytyn K (2008). Identification of ciliary localization sequences within the third intracellular loop of G protein-coupled receptors. Molecular Biology of the Cell, 19(4), 1540–1547. 10.1091/mbc.E07-09-0942. [PubMed: 18256283]

Breslow DK, Koslover EF, Seydel F, Spakowitz AJ, & Nachury MV (2013). An in vitro assay for entry into cilia reveals unique properties of the soluble diffusion barrier. The Journal of Cell Biology, 203(1), 129–147. 10.1083/jcb.201212024. [PubMed: 24100294]

Brini M, Pasti L, Bastianutto C, Murgia M, Pozzan T, & Rizzuto R (1994). Targeting of aequorin for calcium monitoring in intracellular compartments. Journal of Bioluminescence and Chemiluminescence, 9(3), 177–184. 10.1002/bio.1170090312. [PubMed: 7942123]

Brown DC, & Larson RS (2001). Improvements to parallel plate flow chambers to reduce reagent and cellular requirements. BMC Immunology, 2(9). 10.1186/1471-2172-2-9.

Chen T-W, Wardill TJ, Sun Y, Pulver SR, Renninger SL, Baohan A, et al. (2013). Ultrasensitive fluorescent proteins for imaging neuronal activity. Nature, 499(7458), 295–300. 10.1038/nature12354. [PubMed: 23868258]

Christensen ST, Clement CA, Satir P, & Pedersen LB (2012). Primary cilia and coordination of receptor tyrosine kinase (RTK) signalling. The Journal of Pathology, 226(2), 172–184. 10.1002/path.3004. [PubMed: 21956154]

Cobbold PH, & Rink TJ (1987). Fluorescence and bioluminescence measurement of cytoplasmic free calcium. The Biochemical Journal, 248(2), 313–328. Retrieved from http://www.ncbi.nlm.nih.gov/pubmed/3325037. [PubMed: 3325037]

DeCaen PG, Delling M, Vien TN, & Clapham DE (2013). Direct recording and molecular identification of the calcium channel of primary cilia. Nature, 504(7479), 315–318. 10.1038/nature12832. [PubMed: 24336289]

Delling M, Indzhykulian AA, Liu X, Li Y, Xie T, Corey DP, & Clapham DE (2016). Primary cilia are not calcium-responsive mechanosensors. Nature, 531(7596), 656–660. 10.1038/nature17426. [PubMed: 27007841]

Delmas P, Nomura H, Li X, Lakkis M, Luo Y, Segal Y, et al. (2002). Constitutive activation of G-proteins by polycystin-1 is antagonized by polycystin-2. The Journal of Biological Chemistry, 277, 11276–11283. 10.1074/jbc.M110483200. [PubMed: 11786542]

Delous M, Baala L, Salomon R, Laclef C, Vierkotten J, Tory K, et al. (2007). The ciliary gene RPGRIP1L is mutated in cerebello-oculo-renal syndrome (Joubert syndrome type B) and Meckel syndrome. Nature Genetics, 39(7), 875–881. 10.1038/ng2039. [PubMed: 17558409]

Ebashi S, & Endo M (1968). Calcium ion and muscle contraction. Progress in Biophysics and Molecular Biology, 18, 123–183. Retrieved from http://www.ncbi.nlm.nih.gov/pubmed/4894870. [PubMed: 4894870]

Falcone JC, Kuo L, & Meininger GA (1993). Endothelial cell calcium increases during flow-induced dilation in isolated arterioles. The American Journal of Physiology, 264(2 Pt. 2), H653–H659. 10.1152/ajpheart.1993.264.2.H653. [PubMed: 8447477]

Filippin L, Abad MC, Gastaldello S, Magalhães PJ, Sandonà D, & Pozzan T (2005). Improved strategies for the delivery of GFP-based Ca2+ sensors into the mitochondrial matrix. Cell Calcium, 37(2), 129–136. 10.1016/j.ceca.2004.08.002. [PubMed: 15589993]

Fliegauf M, Horvath J, von Schnakenburg C, Olbrich H, Müller D, Thumfart J, et al. (2006). Nephrocystin specifically localizes to the transition zone of renal and respiratory cilia and photoreceptor connecting cilia. Journal of the American Society of Nephrology, 17(9), 2424–2433. 10.1681/ASN.2005121351. [PubMed: 16885411]

Follit JA, Li L, Vucica Y, & Pazour GJ (2010). The cytoplasmic tail of fibrocystin contains a ciliary targeting sequence. The Journal of Cell Biology, 188(1), 21–28. 10.1083/jcb.200910096. [PubMed: 20048263]

Forder J, Scriabine A, & Rasmussen H (1985). Plasma membrane calcium flux, protein kinase C activation and smooth muscle contraction. The Journal of Pharmacology and Experimental Therapeutics, 235(2), 267–273. Retrieved from http://www.ncbi.nlm.nih.gov/pubmed/2414429. [PubMed: 2414429]

Gilula NB, & Satir P (1972). The ciliary necklace. A ciliary membrane specialization. The Journal of Cell Biology, 53(2), 494–509. Retrieved from http://www.pubmedcentral.nih.gov/articlerender.fcgi?artid=2108734&tool=pmcentrez&rendertype=abstract. [PubMed: 4554367]

Griesbeck O, Baird GS, Campbell RE, Zacharias DA, & Tsien RY (2001). Reducing the environmental sensitivity of yellow fluorescent protein. Mechanism and applications. The Journal of Biological Chemistry, 276, 29188–29194. 10.1074/jbc.M102815200. [PubMed: 11387331]

Hanaoka K, Qian F, Boletta A, Bhunia AK, Piontek K, Tsiokas L, et al. (2000). Co-assembly of polycystin-1 and −2 produces unique cation-permeable currents. Nature, 408(6815), 990–994. 10.1038/35050128. [PubMed: 11140688]

Haycraft CJ, Banizs B, Aydin-Son Y, Zhang Q, Michaud EJ, & Yoder BK (2005). Gli2 and Gli3 localize to cilia and require the intraflagellar transport protein polaris for processing and function. PLoS Genetics, 1(4), e53 10.1371/journal.pgen.0010053. [PubMed: 16254602]

Hu Q, Milenkovic L, Jin H, Scott MP, Nachury MV, Spiliotis ET, et al. (2010). A septin diffusion barrier at the base of the primary cilium maintains ciliary membrane protein distribution. Science, 329(5990), 436–439. 10.1126/science.1191054. [PubMed: 20558667]

Huang P, & Schier AF (2009). Dampened Hedgehog signaling but normal Wnt signaling in zebrafish without cilia. Development, 136(18), 3089–3098. 10.1242/dev.041343. [PubMed: 19700616]

Ishikawa H, Thompson J, Yates JR, Marshall WF, & Marshall WF (2012). Proteomic analysis of mammalian primary cilia. Current Biology: CB, 22(5), 414–419. 10.1016/j.cub.2012.01.031. [PubMed: 22326026]

Jin X, Mohieldin AM, Muntean BS, Green JA, Shah JV, Mykytyn K, et al. (2014). Cilioplasm is a cellular compartment for calcium signaling in response to mechanical and chemical stimuli. Cellular and Molecular Life Sciences: CMLS, 71(11), 2165–2178. 10.1007/s00018-013-1483-1. [PubMed: 24104765]

Johns A, Lategan TW, Lodge NJ, Ryan US, Van Breemen C, & Adams DJ (1987). Calcium entry through receptor-operated channels in bovine pulmonary artery endothelial cells. Tissue and Cell, 19(6), 733–745. 10.1016/0040-8166(87)90015-2. [PubMed: 2449744]

Kathem SH, Mohieldin AM, Abdul-Majeed S, Ismail SH, Altaei QH, Alshimmari IK, et al. (2014). Ciliotherapy: A novel intervention in polycystic kidney disease. Journal of Geriatric Cardiology: JGC, 11(1), 63–73. 10.3969/j.issn.1671-5411.2014.01.001. [PubMed: 24748884]

Kerr R, Lev-Ram V, Baird G, Vincent P, Tsien RY, & Schafer WR (2000). Optical imaging of calcium transients in neurons and pharyngeal muscle of C. elegans. Neuron, 26(3), 583–594. 10.1016/S0896-6273(00)81196-4. [PubMed: 10896155]

Lee KL, Guevarra MD, Nguyen AM, Chua MC, Wang Y, & Jacobs CR (2015). The primary cilium functions as a mechanical and calcium signaling nexus. Cilia, 4, 7 10.1186/s13630-015-0016-y. [PubMed: 26029358]

Liem KF, Ashe A, He M, Satir P, Moran J, Beier D, et al. (2012). The IFT-A complex regulates Shh signaling through cilia structure and membrane protein trafficking. The Journal of Cell Biology, 197(6), 789–800. 10.1083/jcb.201110049. [PubMed: 22689656]

Malone AMD, Anderson CT, Tummala P, Kwon RY, Johnston TR, Stearns T, et al. (2007). Primary cilia mediate mechanosensing in bone cells by a calcium-independent mechanism. Proceedings of the National Academy of Sciences of the United States of America, 104(33), 13325–13330. 10.1073/pnas.0700636104. [PubMed: 17673554]

Mank M, Santos AF, Direnberger S, Mrsic-Flogel TD, Hofer SB, Stein V, et al. (2008). A genetically encoded calcium indicator for chronic in vivo two-photon imaging. Nature Methods, 5, 805–811. 10.1038/nmeth.1243. [PubMed: 19160515]

Masyuk AI, Masyuk TV, Splinter PL, Huang BQ, Stroope AJ, & LaRusso NF (2006). Cholangiocyte cilia detect changes in luminal fluid flow and transmit them into intracellular Ca2+ and cAMP signaling. Gastroenterology, 131(3), 911–920. 10.1053/j.gastro.2006.07.003. [PubMed: 16952559]

Miyawaki A, Llopis J, Heim R, Michael McCaffery J, Adams JA, Ikura M, et al. (1997). Fluorescent indicators for Ca2+ based on green fluorescent proteins and calmodulin. Nature, 388, 882–887. 10.1038/42264. [PubMed: 9278050]

Mollet G, Silbermann F, Delous M, Salomon R, Antignac C, & Saunier S (2005). Characterization of the nephrocystin/nephrocystin-4 complex and subcellular localization of nephrocystin-4 to primary cilia and centrosomes. Human Molecular Genetics, 14(5), 645–656. 10.1093/hmg/ddi061. [PubMed: 15661758]

Mukhopadhyay S, Wen X, Chih B, Nelson CD, Lane WS, Scales SJ, et al. (2010). TULP3 bridges the IFT-A complex and membrane phosphoinositides to promote trafficking of G protein-coupled receptors into primary cilia. Genes & Development, 24(19), 2180–2193. 10.1101/gad.1966210. [PubMed: 20889716]

Nagai T, Sawano A, Park ES, & Miyawaki A (2001). Circularly permuted green fluorescent proteins engineered to sense Ca2+. Proceedings of the National Academy of Sciences of the United States of America, 98, 3197–3202. 10.1073/pnas.051636098. [PubMed: 11248055]

Nagai T, Yamada S, Tominaga T, Ichikawa M, & Miyawaki A (2004). Expanded dynamic range of fluorescent indicators for Ca2+ by circularly permuted yellow fluorescent proteins. Proceedings of the National Academy of Sciences of the United States of America, 101, 10554–10559. 10.1073/pnas.0400417101. [PubMed: 15247428]

Nakai J, Ohkura M, & Imoto K (2001). A high signal-to-noise Ca2+ probe composed of a single green fluorescent protein. Nature Biotechnology, 19(2), 137–141. 10.1038/84397.

Nauli SM, Alenghat FJ, Luo Y, Williams E, Vassilev P, Li X, et al. (2003). Polycystins 1 and 2 mediate mechanosensation in the primary cilium of kidney cells. Nature Genetics, 33(2), 129–137. 10.1038/ng1076. [PubMed: 12514735]

Nauli SM, Jin X, AbouAlaiwi WA, El-Jouni W, Su X, & Zhou J (2013). Non-motile primary cilia as fluid shear stress mechanosensors. Methods in Enzymology, 525, 1–20. 10.1016/B978-0-12-397944-5.00001-8. [PubMed: 23522462]

Nauli SM, Kawanabe Y, Kaminski JJ, Pearce WJ, Ingber DE, & Zhou J (2008). Endothelial cilia are fluid shear sensors that regulate calcium signaling and nitric oxide production through polycystin-1. Circulation, 117(9), 1161–1171. 10.1161/CIRCULATIONAHA.107.710111. [PubMed: 18285569]

Nauli SM, Pala R, & Kleene SJ (2016). Calcium channels in primary cilia. Current Opinion in Nephrology and Hypertension, 25(5), 452–458. 10.1097/MNH.0000000000000251. [PubMed: 27341444]

Nauli SM, Sherpa RT, Reese CJ, & Nauli AM (2016). Mechanosensory and chemosensory primary cilia in ciliopathy and ciliotherapy In Rawlinson SCF (Ed.), Mechanobiology (pp. 75–99). Hoboken, NJ: John Wiley & Sons, Inc 10.1002/9781118966174.ch5.

Otto EA, Loeys B, Khanna H, Hellemans J, Sudbrak R, Fan S, et al. (2005). Nephrocystin-5, a ciliary IQ domain protein, is mutated in senior-Loken syndrome and interacts with RPGR and calmodulin. Nature Genetics, 37(3), 282–288. 10.1038/ng1520. [PubMed: 15723066]

Otto EA, Schermer B, Obara T, O'Toole JF, Hiller KS, Mueller AM, et al. (2003). Mutations in INVS encoding inversin cause nephronophthisis type 2, linking renal cystic disease to the function of primary cilia and left-right axis determination. Nature Genetics, 34(4), 413–420. 10.1038/ng1217. [PubMed: 12872123]

Pala R, Mohieldin AM, Shamloo K, Sherpa RT, Kathem SH, Zhou J, et al. (2018). Personalized nanotherapy by specifically targeting cell organelles to improve vascular hypertension. Nano Letters, 19(2), 904–914. 10.1021/acs.nanolett.8b04138. [PubMed: 30582331]

Palmer AE, Giacomello M, Kortemme T, Hires SA, Lev-Ram V, Baker D, et al. (2006). Ca2+ indicators based on computationally redesigned calmodulin-peptide pairs. Chemistry and Biology, 13, 521–530. 10.1016/j.chembiol.2006.03.007. [PubMed: 16720273]

Palmer AE, Jin C, Reed JC, & Tsien RY (2004). Bcl-2-mediated alterations in endoplasmic reticulum Ca2+ analyzed with an improved genetically encoded fluorescent sensor. Proceedings of the National Academy of Sciences of the United States of America, 101, 17404–17409. 10.1073/pnas.0408030101. [PubMed: 15585581]

Pazour GJ, Agrin N, Leszyk J, & Witman GB (2005). Proteomic analysis of a eukaryotic cilium. The Journal of Cell Biology, 170(1), 103–113. 10.1083/jcb.200504008. [PubMed: 15998802]

Pazour GJ, Dickert BL, & Witman GB (1999). The DHC1b (DHC2) isoform of cytoplasmic dynein is required for flagellar assembly. The Journal of Cell Biology, 144(3), 473–481. Retrieved from http://www.ncbi.nlm.nih.gov/pubmed/9971742. [PubMed: 9971742]

Pérez Koldenkova V, & Nagai T (2013). Genetically encoded Ca2+ indicators: Properties and evaluation. Biochimica et Biophysica Acta—Molecular Cell Research, 1833, 1787–1797. 10.1016/j.bbamcr.2013.01.011.

Praetorius HA, & Spring KR (2001). Bending the MDCK cell primary cilium increases intracellular calcium. The Journal of Membrane Biology, 184(1), 71–79. 10.1007/s00232-001-0075-4. [PubMed: 11687880]

Praetorius HA, & Spring KR (2003). Removal of the MDCK cell primary cilium abolishes flow sensing. Journal of Membrane Biology, 191(1), 69–76. 10.1007/s00232-002-1042-4. [PubMed: 12532278]

Romoser VA, Hinkle PM, & Persechini A (1997). Detection in living cells of Ca2+-dependent changes in the fluorescence emission of an indicator composed of two green fluorescent protein variants linked by a calmodulin-binding sequence. A new class of fluorescent indicators. The Journal of Biological Chemistry, 272(20), 13270–13274. Retrieved from http://www.ncbi.nlm.nih.gov/pubmed/9148946. [PubMed: 9148946]

Rudolf R, Mongillo M, Rizzuto R, & Pozzan T (2003). Looking forward to seeing calcium. Nature Reviews. Molecular Cell Biology, 4(7), 579–586. 10.1038/nrm1153. [PubMed: 12838340]

Sabatini BL, Oertner TG, & Svoboda K (2002). The life cycle of Ca2+ ions in dendritic spines. Neuron, 33(3), 439–452. 10.1016/S0896-6273(02)00573-1. [PubMed: 11832230]

Satir P (2017). CILIA: Before and after. Cilia, 6(1), 1 10.1186/s13630-017-0046-8. [PubMed: 28293419]

Schou KB, Pedersen LB, & Christensen ST (2015). Ins and outs of GPCR signaling in primary cilia. EMBO Reports, 16(9), 1099–1113. 10.15252/embr.201540530. [PubMed: 26297609]

Singla V, & Reiter JF (2006). The primary cilium as the cell's antenna: Signaling at a sensory organelle. Science (New York, N.Y.), 313(5787), 629–633. 10.1126/science.1124534.

Sorokin S (1962). Centrioles and the formation of rudimentary cilia by fibroblasts and smooth muscle cells. The Journal of Cell Biology, 15(2), 363–377. 10.1083/jcb.15.2.363. [PubMed: 13978319]

Sorokin SP (1968). Reconstructions of centriole formation and ciliogenesis in mammalian lungs. Journal of Cell Science, 3(2), 207–230. Retrieved from http://www.ncbi.nlm.nih.gov/pubmed/5661997. [PubMed: 5661997]

Souslova EA, Belousov VV, Lock JG, Strömblad S, Kasparov S, Bolshakov AP, et al. (2007). Single fluorescent protein-based Ca2+ sensors with increased dynamic range. BMC Biotechnology, 7(1), 37 10.1186/1472-6750-7-37. [PubMed: 17603870]

Su S, Phua SC, Derose R, Chiba S, Narita K, Kalugin PN, et al. (2013). Genetically encoded calcium indicator illuminates calcium dynamics in primary cilia. Nature Methods, 10, 1105–1107. 10.1038/nmeth.2647. [PubMed: 24056873]

Tian L, Hires SA, Mao T, Huber D, Chiappe ME, Chalasani SH, et al. (2009). Imaging neural activity in worms, flies and mice with improved GCaMP calcium indicators. Nature Methods, 6(12), 875–881. 10.1038/nmeth.1398. [PubMed: 19898485]

Valente EM, Logan CV, Mougou-Zerelli S, Lee JH, Silhavy JL, Brancati F, et al. (2010). Mutations in TMEM216 perturb ciliogenesis and cause Joubert, Meckel and related syndromes. Nature Genetics, 42(7), 619–625. 10.1038/ng.594. [PubMed: 20512146]

Wier W, Cannell M, Berlin M, Marban E, & Lederer W (1987). Cellular and subcellular heterogeneity of [Ca2+]i in single heart cells revealed by fura-2. Science, 235(4786), 325–328. 10.1126/science.3798114. [PubMed: 3798114]

Williams DA, Fogarty KE, Tsien RY, & Fay FS (1985). Calcium gradients in single smooth muscle cells revealed by the digital imaging microscope using Fura-2. Nature, 318(6046), 558–561. 10.1038/318558a0. [PubMed: 3934562]

Williams CL, Masyukova SV, & Yoder BK (2010). Normal ciliogenesis requires synergy between the cystic kidney disease genes MKS-3 and NPHP-4. Journal of the American Society of Nephrology, 21(5), 782–793. 10.1681/ASN.2009060597. [PubMed: 20150540]

Williams CL, Winkelbauer ME, Schafer JC, Michaud EJ, & Yoder BK (2008). Functional redundancy of the B9 proteins and nephrocystins in *Caenorhabditis elegans* ciliogenesis. Molecular Biology of the Cell, 19(5), 2154–2168. 10.1091/mbc.e07-10-1070. [PubMed: 18337471]

Xu C, Rossetti S, Jiang L, Harris PC, Brown-Glaberman U, Wandinger-Ness A, et al. (2006). Human ADPKD primary cyst epithelial cells with a novel, single codon deletion in the PKD1 gene exhibit defective ciliary polycystin localization and loss of flow-induced Ca2+ signaling. AJP: Renal Physiology, 292(3), F930–F945. 10.1155/2013/715848. [PubMed: 17090781]

Yuan S, Zhao L, Brueckner M, & Sun Z (2015). Intraciliary calcium oscillations initiate vertebrate left-right asymmetry. Current Biology, 25(5), 556–567. 10.1016/j.cub.2014.12.051. [PubMed: 25660539]

Zhao Y, Araki S, Wu J, Teramoto T, Chang YF, Nakano M, et al. (2011). An expanded palette of genetically encoded Ca2+ indicators. Science. 10.1126/science.1208592.

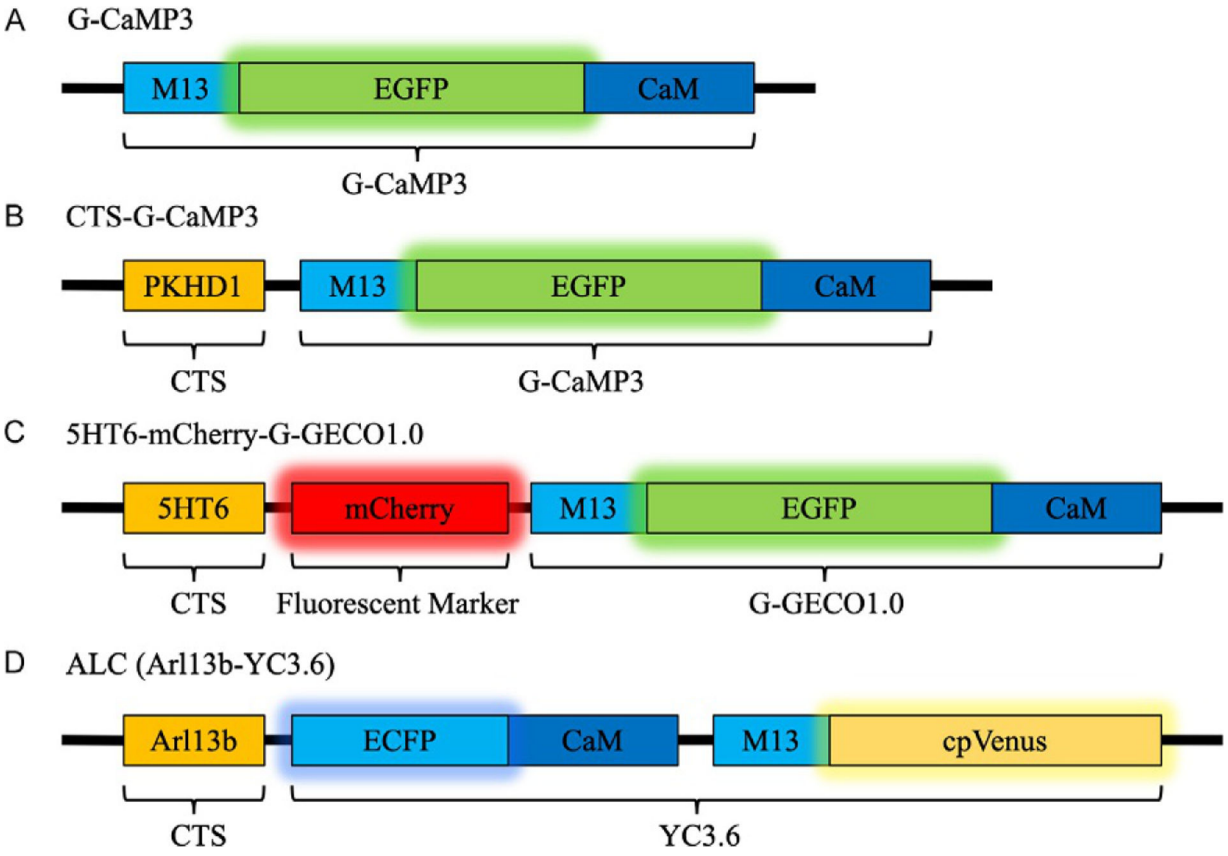

FIG. 1.

Schematic representation of GECI construct. (A) G-CaMP3 is a single fluorescent Ca^{2+} sensor and after fusion with CTS such as the cytoplasmic tail of PKHD1 in (B) CTS-G-CaMP3, the sensor localizes to the cilioplasm. (C) In 5HT6-mCherry-G-GECO1.0 the Ca^{2+} sensor, G-GECO1.0 is attached to a CTS derived from 5HT6 and mCherry, a stable fluorescence marker to track ciliary movement. (D) ALC is another GECI based on FRET for Ca^{2+} quantification, fused with the CTS Arl13b for cilia localization.

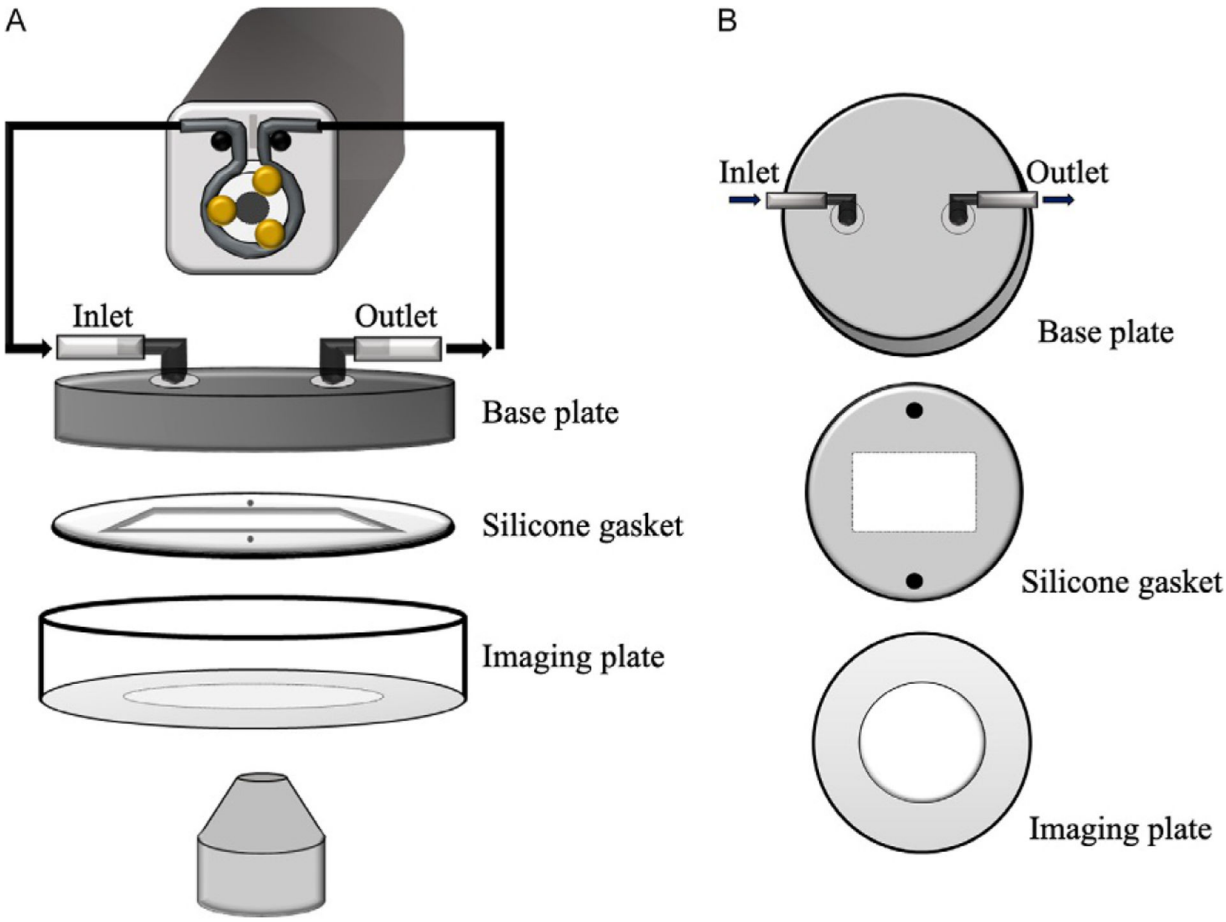

FIG. 2.

Flow equipment setup for live cell and cilia imaging. (A) The flow setup uses a peristaltic pump in a closed loop system. The perfusion chamber consists of a top base plate with inlet and outlet connected to the pump. Then we have a silicone gasket to form a channel for laminar flow and finally, a glass bottom imaging plate. (B) Top view of each perfusion chamber component.

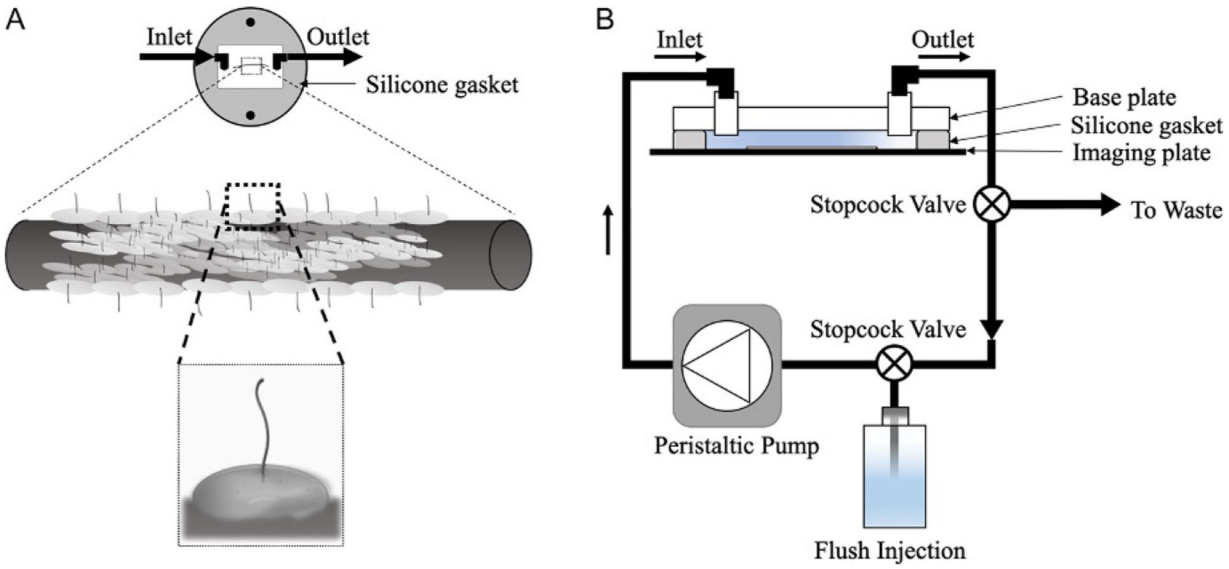

FIG. 3.

Microwire with cells in a perfusion chamber. (A) In the diagram, the gasket is placed on the imaging dish in a manner to orient the microwire parallel to laminar flow. Using lower magnifications, we can observe cells growing on the wire edge. At a higher magnification, the cilium protruding outward should become even clearer. We will focus on a single cell and capture Ca^{2+} data in response to fluid flow. (B) Schematic of the experimental setup with stopcock valves to load and unload buffers into circulation.

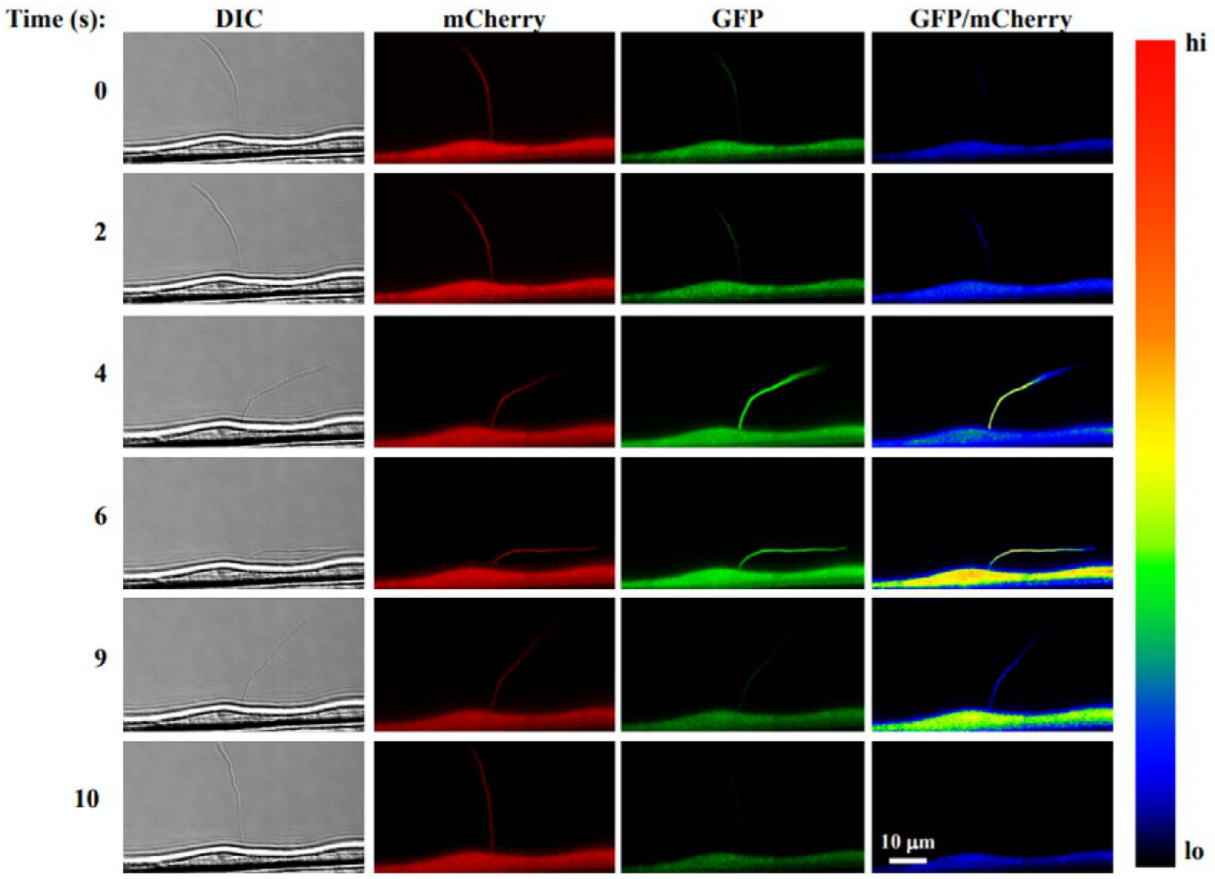

FIG. 4.

Single-live cell and cilia imaging with 5HT6-mCherry-G-GECO1.0. The images show (from left to right column) DIC used for tracking a cilium, mCherry fluorescent ciliary marker, the Ca^{2+} sensitive GECO1.0 and an EGFP/mCherry ratio pseudocolored to show Ca^{2+} levels. When fluid flow is applied (time series from top to bottom), the cilium bends inducing a Ca^{2+} increase in both the cytoplasm and cilioplasm.

Adapted with permission from Pala, R., Mohieldin, A. M., Shamloo, K., Sherpa, R. T., Kathem, S. H., Zhou, J., et al. Personalized nanotherapy by specifically targeting cell organelles to improve vascular hypertension. Nano Letters, 19, 904–914. Copyright 2018 American Chemical Society.

Table 1

Properties of some G-CAMP based sensors and their cilia targeting derivatives.

Name	DR[a]	K_d (Ca^{2+}) (nM)	Comments	References
General cytosolic GECI				
G-CaMP	4.3 ×	235	Weak fluorescence at physiological temperatures compared to EGFP	Souslova et al. (2007) Nakai et al. (2001)
G-CaMP3	12 ×	540	1.3 × higher affinity to Ca^{2+} and 3 × more dynamic range compared to G-CaMP	Zhao et al. (2011)
G-GECO1.0	25 ×	750	2 × higher dynamic range compared to G-CaMP3	Zhao et al. (2011) Pala et al. (2018)
G-GECO1.2	23 ×	1150	Sensitive to a range of 1–10 μM Ca^{2+}	Zhao et al. (2011)
G-CaMP6s	23 ×	144	10 × higher sensitivity and increased dynamic range than G-CaMP3	Chen et al. (2013)
Cilia targeting GECI				
Arl13b-G-CaMP6	23 ×	144	Arl13b is used to localize G-CaMP6 to the cilioplasm	Yuan, Zhao, Brueckner, and Sun (2015) Chen et al. (2013)
ALC (Arl13b fused to YC3.6)	5.6 ×	250	FRET-based sensor with ECFP & cpVenus (donor-acceptor)	Lee et al. (2015) Nagai, Yamada, Tominaga, Ichikawa, and Miyawaki (2004)
Arl13b-mCherry-GECO1.2	–	450	Reaches saturation at 800 nM Ca^{2+}	Delling et al. (2016)
CTS-G-CaMP3	12 ×	542	Contains the intracellular C-tail of fibrocystin, Pkhd1 (C1–68) for ciliary localization of the sensor	Jin et al. (2014)
5HT6-mCherry-G-GECO1.0	25 ×	750	mCherry allows constant cilia fluorescence and ratiometric analysis	Su et al. (2013) Pala et al. (2018)

[a]Dynamic Range (DR) is defined as the ratio of emission intensities ($\Delta F/F_0$) for intensiometric GECOs and the ratio of emission ratios ($\Delta EGFP/EGFP_0$)/($\Delta mCherry/mCherry_0$) for 5HT6-mCherry-G-GECO1.0. For ALC, the dynamic range is derived from (E_{max} E_{min})/E_{min}, where E is FRET efficiency.